

# Photonic Berry curvature in double liquid crystal microcavities with broken inversion symmetry

P. Kokhanchik,<sup>1</sup> H. Sigurdsson,<sup>1,2</sup> B. Piętko,<sup>3</sup> J. Szczytko,<sup>3</sup> and P.G. Lagoudakis<sup>1,2,\*</sup>

<sup>1</sup>Skolkovo Institute of Science and Technology, Bolshoy Boulevard 30, bld. 1, Moscow, 121205, Russia  
<sup>2</sup>School of Physics and Astronomy, University of Southampton, Southampton SO17 1BJ, United Kingdom

<sup>3</sup>Institute of Experimental Physics, Faculty of Physics,  
 University of Warsaw, ul. Pasteura 5, PL-02-093 Warsaw, Poland

(Dated: September 16, 2020)

We investigate a photonic device consisting of two coupled cavities possessing a Rashba-Dresselhaus spin-orbit coupling, a TE-TM and a controllable XY polarisation energy splitting that open a tuneable energy gap at the diabolic points of the photon dispersion; the latter giving rise to an actively addressable local Berry curvature. The proposed architecture stems from recent advancements in the design of artificial photonic gauge fields in liquid crystal cavities [K. Rechcińska et al., *Science* **366**, 727 (2019)]. Our study opens new perspectives for topological photonics, room-temperature spinoptronics, and studies on the quantum geometrical structure of photonic bands in extreme settings.

*Introduction* — Shaping and molding the optical properties in structured microscale systems (e.g., photonic crystals) has both wide and important impact in quantum optics, information transfer, light-matter interactions, and for future optoelectronic and spinoptronic devices [1]. Perhaps one of the most promising outcomes of engineering cavity photon dispersions is access to photonic analogues of electronic solid state physics where the role of the electron spin is instead played by the vectorial composition of the photon polarization. Indeed, designing artificial gauge fields for photons [2] has resulted in a surge of research dedicated to topological photonics [3, 4] and synthesis of photonic spin-orbit coupling (SOC) Hamiltonians [5–7] in a similar spirit to advancements in cold atoms [8] and solids [9].

Recently, flexible liquid crystal (LC) microcavities have displayed an amazing ability to tune their cavity photon dispersions between the TE and TM polarized modes, realizing synthetic spin-orbit coupling of light [10, 11]. The flexibility stems from the voltage dependent orientation of the LC molecular director allowing one to control the dielectric tensor of the cavity by adjusting the voltage applied to the LC. Moreover, since LC cavities operate at room-temperature conditions they are highly favorable in bringing complex applied photonic architectures reliant on artificial gauge fields, and topological photonics, closer to commercial use.

With this development, a new generation of devices can be constructed of compound cavity systems which hybridize distinct gauge fields in different cavities to produce more exotic photonic gauge fields (see Fig. 1a). Double microcavity systems have already been studied in both the weak coupling regime (i.e., photon lasing) [12–14] and in the strong-coupling regime (e.g., by using embedded semiconductor quantum wells in the cavities) [15, 16]. Of interest, it was shown [17] in strongly coupled systems that the emergent exciton-polaritons quasiparticles possessed excitation power-dependent spin textures appearing from interplay between their inherited photonic SOC and exciton-exciton interactions. Although many-body physics in such compound systems can give new complex spin dynamics and effective magnetic fields (e.g., the self-induced Larmor precession [18]) it is unpractical in a pure

photonic setting where particle nonlinearities are weak. On the other hand, given their recent development, compound LC cavity systems have not been considered until now to provide access to new photonic gauge field physics.

In this Letter we demonstrate how a simple system of two coupled microcavities containing LCs, as shown in Fig. 1a, each possessing different SOC mechanisms give rise to a gap opening at photonic Dirac points [19, 20] with the formation of non-zero local Berry curvature [21] which quantifies important physical properties like the Chern number and intrinsic anomalous Hall conductivity in electron systems.

We consider a double microcavity like shown in Fig. 1a where both cavities are filled with a LC. We will define the cavity light Stokes components in the basis of circular polarization of the cavity field  $\Psi = (\psi_+, \psi_-)^t$ . The Stokes components then become  $S_1 = \text{Re}(\psi_+ \psi_-^*)$ ,  $S_2 = -\text{Im}(\psi_+ \psi_-^*)$ ,  $S_3 = (|\psi_+|^2 - |\psi_-|^2)/2$ ,  $S = (|\psi_+|^2 + |\psi_-|^2)/2$ . From here on we will work with the normalized Stokes components  $S_n \rightarrow S_n/S$ . The birefringence of the LC in the notation given in Fig. 1 is written  $\Delta n_i = n_{ei} - n_{oi}$  where  $i$  denotes the cavity in question. The effective refractive index for x-polarized light is written:

$$n_{\text{eff},i} = \frac{n_{oi}n_{ei}}{\sqrt{n_{oi}^2 \cos^2(\varphi_i) + n_{ei}^2 \sin^2(\varphi_i)}}, \quad (1)$$

while for y-polarized light refractive index is always equal  $n_{oi}$  for the  $i$ th cavity. For normal incident light of wavelength  $\lambda$  the resonance condition for horizontal and vertical polarized light (along the  $x$  and  $y$  axis respectively) can be written,

$$m_{xi} = \frac{2d_i n_{\text{eff},i}}{\lambda}, \quad m_{yi} = \frac{2d_i n_{oi}}{\lambda}, \quad (2)$$

where  $d_i$  denotes the  $i$ th cavity size.

It was recently shown that a photonic equivalent of the Rashba and Dresselhaus (RD) SOC can be synthesized in a single LC cavity [11] through voltage dependent tuning of its LC director. There, cavity modes of orthogonal polarizations and opposite parity were tuned into resonance by rotating the molecular director such that their coupling resulted in

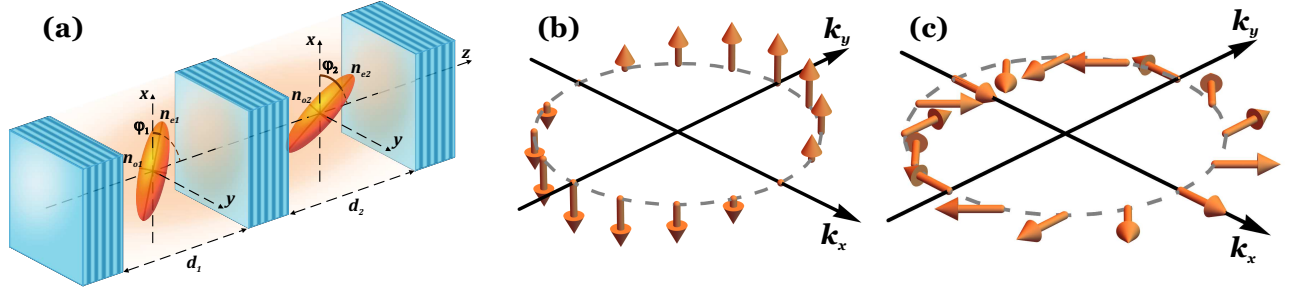


FIG. 1. **Scheme of the double microcavity system and the effective magnetic fields.** (a) In each cavity, the ellipsoid of a refractive index is drawn and notations are introduced. Blue-ish stacked layers indicate the dielectric Bragg reflectors (DBRs). The ordinary and extraordinary refractive indices of the LC are denoted by  $n_{oi}$  and  $n_{ei}$  in the  $i$ th cavity. Panels (b) and (c) represent effective Rashba-Dresselhaus and optical spin Hall effect induced magnetic fields respectively, as orange arrows in momentum space not taking into account the static  $XY$  splitting term for the optical spin Hall effect field ( $\beta = 0$ ).

an effective RD SOC for the cavity photons. Here, the LC filled cavity in our double cavity system is taken to possess a RD Hamiltonian which, in reciprocal-space representation and circular polarization basis, is written:

$$\hat{H}_{\text{RD}} = \frac{\hbar^2 k_x^2}{2M_x} + \frac{\hbar^2 k_y^2}{2M_y} - 2\alpha k_y \hat{\sigma}_z. \quad (3)$$

Here,  $\hat{\sigma}_{x,y,z}$  are the Pauli matrices,  $M_{x,y}$  is the cavity photon mass along the  $x$  and  $y$  planar coordinates,  $k_{x,y} = k(\cos(\varphi), \sin(\varphi))$  are the in-plane momenta, and  $\alpha$  is the strength of the RD SOC. The Hamiltonian in Eq. (3) can be represented as a linear combination of a Pauli matrices vector and an effective magnetic field:

$$\hat{H}_{\text{RD}} = \frac{\hbar^2 k_x^2}{2M_x} + \frac{\hbar^2 k_y^2}{2M_y} + \mathbf{B}^{\text{RD}} \cdot \hat{\boldsymbol{\sigma}}, \quad (4)$$

where  $\hat{\boldsymbol{\sigma}} = (\hat{\sigma}_x; \hat{\sigma}_y; \hat{\sigma}_z)$  is a vector of Pauli matrices which relates to the cavity photon pseudospin through  $\mathbf{S} = \langle \hat{\boldsymbol{\sigma}} \rangle$ , and  $\mathbf{B}^{\text{RD}} = (0; 0; -2\alpha k_y)$  is the effective RD magnetic field (Fig. 1b).

On the other hand, the second cavity in our double LC cavity system is taken to possess two polarization dependent mechanisms in correspondence with recent studies [10, 11]. First, a splitting between the TE and TM polarized modes which results in a unique photonic SOC described by an effective in-plane magnetic field which winds itself twice around the momentum space origin, whereas, in comparison, Rashba and Dresselhaus SOC's wind only once. The TE-TM splitting results in the optical spin Hall effect (OSHE) [22] and is a source of multiple interesting features relevant to topological photonics [19, 23, 24]. Second, a static splitting term between the linearly polarized modes of the photons (referred here as a  $XY$  splitting). Such cavity can be described by the Hamiltonian:

$$\hat{H}_{\text{OSHE}} = \begin{pmatrix} \frac{\hbar^2 k_x^2}{2M_x} + \frac{\hbar^2 k_y^2}{2M_y} & \beta + \gamma k^2 e^{-i2\varphi} \\ \beta + \gamma k^2 e^{i2\varphi} & \frac{\hbar^2 k_x^2}{2M_x} + \frac{\hbar^2 k_y^2}{2M_y} \end{pmatrix}. \quad (5)$$

The TE-TM and  $XY$  splitting are denoted by  $\gamma$  and  $\beta$  respectively in Eq. (5). Note the  $2\varphi$  dependence indicating the double winding of the effective in-plane magnetic field. Similarly to the representation used in Eq. (4), we can write the OSHE Hamiltonian in the following form:

$$\hat{H}_{\text{RD}} = \frac{\hbar^2 k_x^2}{2M_x} + \frac{\hbar^2 k_y^2}{2M_y} + \mathbf{B}^{\text{OSHE}} \cdot \hat{\boldsymbol{\sigma}}, \quad (6)$$

where  $\mathbf{B}^{\text{OSHE}} = (\beta + \gamma(k_x^2 - k_y^2); 2\gamma k_x k_y; 0)$  is an effective OSHE magnetic field. In Fig. 1c we have depicted OSHE magnetic field for the case  $\beta = 0$ .

As pointed out in recent works [24, 25], the presence of both TE-TM and  $XY$  splitting in a single cavity leads to two energetically shifted parabolas with different effective masses which intersect into two tilted Dirac cones located at  $(k_x, k_y) = (0, \pm\sqrt{\beta/\gamma})$ , also referred as diabolical points (see Fig. 2a). Recently, this Hamiltonian was realized in single microcavity with embedded quantum wells and operating in the strong-coupling regime [24], as well as in polariton microcavity based on an optical birefringent 2D perovskite [26]. There, the emergent spinor polariton modes (two-band system) were then subjected to an external out-of-plane magnetic field described by an operator  $\Omega_z = \Delta \hat{\sigma}_z$  which, when combined with  $\hat{H}_{\text{OSHE}}$  resulted in a gap opening at the Dirac points and formation of non-zero Berry curvature in momentum space.

The fact that each Hamiltonian given by Eq. (3) and (5) can be easily realized in a double cavity setting provides an opportunity to explore a new regime of local photonic Berry curvature. That is, in order to realize a gap opening at the Dirac cones of  $\hat{H}_{\text{OSHE}}$  for just cavity photons, instead of using magnetically susceptible polaritons [24], practically inaccessible in organic microcavities, we propose a four-band system of two coupled cavities,

$$\hat{H} = \begin{pmatrix} \Delta E \hat{\sigma}_0 + \hat{H}_{\text{OSHE}} & V \hat{\sigma}_0 \\ V \hat{\sigma}_0 & \hat{H}_{\text{RD}} \end{pmatrix}. \quad (7)$$

Here,  $\Delta E$  is the detuning between OSHE and RD cavities,  $\hat{\sigma}_0$  is the  $2 \times 2$  identity operator and we have used the simplest model of coupling between the cavities denoted by the

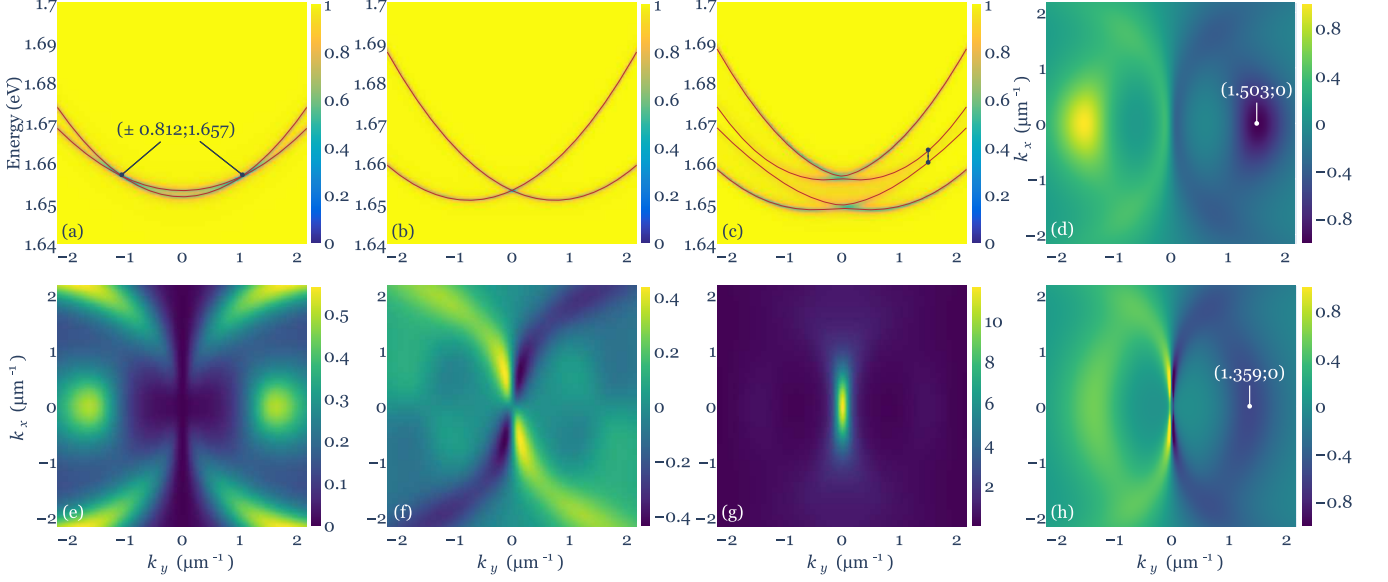


**FIG. 2. Gap opening of the hybridized OSHE and RD double cavity system.** Dispersions (normalized reflection intensities of the diagonally polarized incident light) of the (a) uncoupled OSHE cavity where we mark the parabolas intersection, (b) uncoupled RD cavity, and (c) both cavities coupled calculated using Berreman method [27]. In (a-c) we have plotted the energies coming from Eqs. (5), (3) and (7), respectively, as whole red lines with a vertical marker in (c) indicating the smallest splitting between the central branches. (d) Berry curvature  $B_z$ , QGT components (e)  $g_{xx}$ , (f)  $g_{xy} = g_{yx}$ , (g)  $g_{yy}$ ; (h) Berry curvature  $B_z$  for different LC director angle. Subplots (d-h) are calculated for the second band counted from bottom to top. Parameters for (a-g) are:  $\lambda = 750$  nm,  $n_{o1} = n_{o2} = 1.5$ ,  $\Delta n_1 = \Delta n_2 = 0.4$ ,  $m_{x1} = 3$ ,  $m_{y1} = 3 + 4 \times 10^{-3}$  ( $\varphi_1 = 85.18$  deg),  $m_{x2} = 7$ ,  $m_{y2} = 8$ ,  $N_1 = 10$ ,  $N_2 = 12$ ,  $N_3 = 10$ ,  $n_{DBR1} = 1.4$ ,  $n_{DBR2} = 2.3$ . Parameters for (h) are the same except for  $m_{y1} = 3 + 10^{-4}$  ( $\varphi_1 = 89.24$  deg).

real valued coefficient  $V$  which is taken to be independent of in-plane momentum. The photonic hybridization of the two subsystems  $\hat{H}_{RD}$  and  $\hat{H}_{OSHE}$  can then achieve a similar gap opening and finite local Berry curvature like reported in [24] but with zero Chern number since the system is topologically trivial. Instead of a magnetic field that breaks time-reversal symmetry and opens a gap at the Dirac points our system instead breaks the inversion symmetry through the hybridization of the two cavities. One cavity possesses TE-TM and XY splitting giving rise to Dirac cones in one subsystem, while the other has the RD SOC which, when coupled with the former, breaks inversion symmetry and opens the gap at the Dirac points with consequent emergence of non-zero local Berry curvature [28] in the coupled system. Indeed,  $\hat{H}$  is symmetric under time-reversal whereas it is not for inversion  $\mathcal{I} = \sigma_0 \otimes \sigma_x$ ,

$$\mathcal{I}\hat{H}(-\mathbf{k})\mathcal{I}^{-1} \neq \hat{H}(\mathbf{k}). \quad (8)$$

Before presenting the results for a double LC system, we want to note that a similar symmetry breaking effect can be realized in a simpler system from the point of view of manufacturing, which is a combination of an empty cavity and a LC cavity tuned to the RD Hamiltonian (Eq. (3)). Indeed, an empty cavity can possess TE-TM splitting when the mode is shifted relative to the center of the DBRs stopband [29], and XY splitting can be implemented by creating an asym-

metric microcavity [30], or using slightly detuned RD modes of the LC cavity [11]. In the last case, the Hamiltonian in Eq. (3) would have an additional term  $\beta^* \hat{\sigma}_x$  similar to the one in Eq. (5). However, the experimentally reported TE-TM splitting values for an empty microcavity are of the order of tens of  $\mu\text{eV}$  [31], while the TE-TM splitting values in LC cavity are measured in the meV scale providing comparable scales for  $\alpha, \beta$  and  $\gamma$  values and allowing for an observable gap opening.

In Fig. 2a,b we calculate the dispersion of each uncoupled cavity belonging Eqs. (3) and (5) respectively. The diabolic points, or Dirac cones, are marked with the black lines in Fig. 2a. When the two systems are coupled using Eq. (7) we observe a splitting between the two central bands around the Dirac point which contain non-zero Berry curvature satisfying  $B_z(\mathbf{k}) = -B_z(-\mathbf{k})$ . In order to characterize the properties of the bands in the double cavity system we calculate the components of the quantum geometric tensor [25, 32] (QGT), whose real part contains the quantum metric (distance between eigenstates), and the imaginary part determines the Berry curvature.

$$T_{ij}^{(n)} = \sum_{m \neq n} \frac{\langle m | \partial_{k_i} \hat{H} | n \rangle \langle n | \partial_{k_j} \hat{H} | m \rangle}{(E_m - E_n)^2}, \quad (9)$$

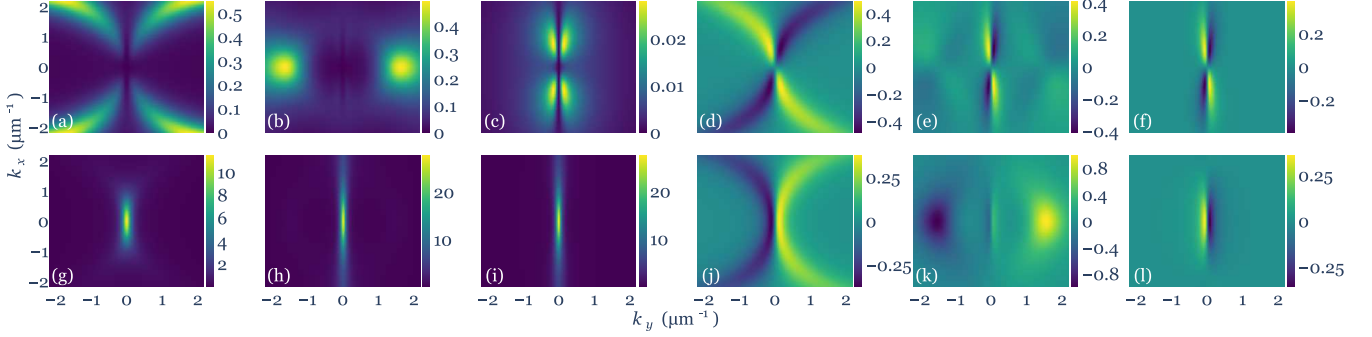


FIG. 3. **Quantum metric tensor components and Berry curvature.** The quantum metric tensor components (a,b,c)  $g_{xx}$ , (d,e,f)  $g_{xy} = g_{yx}$ , (g,h,i)  $g_{yy}$  and (j,k,l) the Berry curvature  $B_z$  for the first (left figure in each subset), the third (middle figure) and the fourth (right figure) bands counted up.

$$g_{ij}^{(n)} = \text{Re} \left( T_{ij}^{(n)} \right), \quad B_z^{(n)} = -2\text{Im} \left( T_{xy}^{(n)} \right), \quad (10)$$

where  $(i, j) = (x, y)$ ,  $n = (1, 2, 3, 4)$  denotes the number of the band from bottom to top in energy,  $|n\rangle$  and  $E_n$  are the  $k$ -dependent eigenstate and corresponding eigenenergy of  $\hat{H}$ .

The QGT components for the second lowest band of this system are shown in the Fig. 2(d-g) revealing that the strongest Berry curvature appears at the anticrossing of the two central bands of the system. Figure 2h shows that this minimum/maximum of the Berry curvature, marked with a white dot, is shifted when the LC director is changed, underlining tunability coming from the LC cavities. In Fig. 2h the colorscale is saturated to match Fig. 2d. The black segment in Fig. 2c shows the anticrossing, marking the opening point of the Dirac cone corresponding to the white point in Fig. 2d. We note that the QGT components for a four-band system can be directly measured [25]. The QGT components for the remaining three bands are shown in Fig. 3.

For all effective masses we use notations  $M_{x1}, M_{y1}, M_{x2}, M_{y2}$ , where indices (1,2) correspond to  $\hat{H}_{\text{OSHE,RD}}$  cavities respectively. In Fig. 2a-c we obtain an XY splitting  $\beta = 0.77 \text{ meV}$ , TE-TM splitting  $\gamma = 0.72 \text{ meV} \cdot \mu\text{m}^2$ , effective photon masses  $M_{x1} = M_{y1} = 0.054 \text{ meV} \cdot \text{ps}^2 \cdot \mu\text{m}^{-2}$ ,  $M_{y2} = 0.05 \text{ meV} \cdot \text{ps}^2 \cdot \mu\text{m}^{-2}$ , cavities detuning  $\Delta E = -0.8 \text{ meV}$ , RD SOC parameter  $\alpha = 3.25 \text{ meV} \cdot \mu\text{m}$ , and the coupling between cavities  $V = 3.6 \text{ meV}$  by fitting to the numerically calculated dispersions (red lines in Fig. 2a-c). The effective mass along the  $k_x$  direction  $M_{x2} = 0.0445 \text{ meV} \cdot \text{ps}^2 \cdot \mu\text{m}^{-2}$  does not affect the gap opening, nor does it affect the position of the Dirac cones, it only affects the width of the distribution of the QGT parameters along the  $k_x$ -axis. It can therefore adopt a typical value obtained using the methods of Ref. [11]. We note that the plotted energies belonging to Eq. (7) are shifted to match the absolute energies obtained through numerics. For the case of all masses being equal and  $k_x = 0$  and  $\Delta E = 0$ , the analytical expression for the energies becomes:

$$E = \frac{\hbar^2 k_y^2}{2M} \pm \sqrt{\frac{2V^2 + 4\alpha^2 k_y^2 + (\beta - \gamma k_y^2)^2 \pm \sqrt{(\beta - \gamma k_y^2)^2 [(\beta - \gamma k_y^2)^2 + 4V^2 - 8\alpha^2 k_y^2] + 16\alpha^2 k_y^2 [V^2 + \alpha^2 k_y^2]}}{2}}. \quad (11)$$

The above expression gives some insight into how the location of the maximum concentration of Berry curvature at the anti-crossing point has shifted with respect to the original Dirac point location  $k_y = \pm\sqrt{\beta/\gamma}$ . To the leading order around the original Dirac point, the new location is given by the roots of the equation,

$$\frac{V^2 + 2\alpha^2 k_y^2}{\sqrt{V^2 + \alpha^2 k_y^2}} = \frac{k_y}{\alpha} (2\alpha^2 - \gamma(\beta - \gamma k_y^2)). \quad (12)$$

The solution satisfies  $|k_y| > \sqrt{\beta/\gamma}$  corresponding to the anti-crossing point shifting to higher momentum values away from the original Dirac point.

*Discussion* — We have demonstrated a purely photonic implementation of achieving measurable local Berry curvature by construction of a Hamiltonian describing two optical cavities possessing distinct SOC mechanisms. These SOC mechanisms can today be readily designed through the recent advancements in tunable LC microcavities [10, 11]. In our proposal, one cavity is composed to a unique photonic SOC effect

stemming from both TE-TM and  $XY$  splitting of the cavity modes leading to a pair of tilted Dirac cones. The second cavity provides an RD SOC which, when coupled with the former cavity, breaks inversion symmetry and leads to gap opening at the Dirac points. The opening is associated with the formation of local Berry curvature around the Dirac points. Our results open new possibilities for measuring fundamental geometrical properties of photonic bands, such as the Berry curvature, which are of great interest to the growing field of topological photonics [4]. Namely, the appearance of local Berry curvature in our system is not reliant on gyromagnetic materials, polariton susceptibility to external magnetic fields, or complicated fabrication of in-plane photonic structures like honeycomb lattices [7, 21].

*Acknowledgements* — The authors acknowledge the support of the Skoltech NGP Program (Skoltech-MIT joint project), the UK's Engineering and Physical Sciences Research Council (Grant No. EP/M025330/1 on Hybrid Polaritonics), and by RFBR according to the research Projects No. 20-52-12026 (jointly with DFG) and No. 20-02-00919, and National Science Centre, Poland grant no. UMO-2019/35/B/ST3/04147.

---

\* [p.lagoudakis@skoltech.ru](mailto:p.lagoudakis@skoltech.ru)

- [1] K. J. Vahala, *Nature* **424**, 839 (2003).
- [2] D. Hey and E. Li, *Royal Society Open Science* **5**, 172447 (2018).
- [3] L. Lu, J. D. Joannopoulos, and M. Soljačić, *Nature Photonics* **8**, 821 (2014).
- [4] T. Ozawa, H. M. Price, A. Amo, N. Goldman, M. Hafezi, L. Lu, M. C. Rechtsman, D. Schuster, J. Simon, O. Zilberberg, and I. Carusotto, *Rev. Mod. Phys.* **91**, 015006 (2019).
- [5] C. Leyder, M. Romanelli, J. P. Karr, E. Giacobino, T. C. H. Liew, M. M. Glazov, A. V. Kavokin, G. Malpuech, and A. Bramati, *Nature Physics* **3**, 628 (2007).
- [6] K. Y. Bliokh, F. J. Rodríguez-Fortuño, F. Nori, and A. V. Zayats, *Nature Photonics* **9**, 796 (2015).
- [7] V. G. Sala, D. D. Solnyshkov, I. Carusotto, T. Jacqmin, A. Lemaître, H. Terças, A. Nalitov, M. Abbarchi, E. Galopin, I. Sagnes, J. Bloch, G. Malpuech, and A. Amo, *Phys. Rev. X* **5**, 011034 (2015).
- [8] J. Dalibard, F. Gerbier, G. Juzeliūnas, and P. Öhberg, *Rev. Mod. Phys.* **83**, 1523 (2011).
- [9] M. Vozmediano, M. Katsnelson, and F. Guinea, *Physics Reports* **496**, 109 (2010).
- [10] K. Lekenta, M. Król, R. Mirek, K. Łempicka, D. Stephan, R. Mazur, P. Morawiak, P. Kula, W. Piecek, P. G. Lagoudakis, B. Piętka, and J. Szczytko, *Light: Science & Applications* **7**, 74 (2018).
- [11] K. Rechcińska, M. Król, R. Mazur, P. Morawiak, R. Mirek, K. Łempicka, W. Bardyszewski, M. Matuszewski, P. Kula, W. Piecek, P. G. Lagoudakis, B. Piętka, and J. Szczytko, *Science* **366**, 727 (2019).
- [12] M. Bayer, T. Gutbrod, J. P. Reithmaier, A. Forchel, T. L. Reinecke, P. A. Knipp, A. A. Dremin, and V. D. Kulakovskii, *Phys. Rev. Lett.* **81**, 2582 (1998).
- [13] S. Michaelis de Vasconcellos, A. Calvar, A. Dousse, J. Sufczyński, N. Dupuis, A. Lemaître, I. Sagnes, J. Bloch, P. Voisin, and P. Senellart, *Applied Physics Letters* **99**, 101103 (2011).
- [14] E. Noble, R. V. Nair, and B. N. Jagatap, *Journal of Modern Optics* **63**, 1981 (2016).
- [15] V. Ardizzone, P. Lewandowski, M. H. Luk, Y. C. Tse, N. H. Kwong, A. Lücke, M. Abbarchi, E. Baudin, E. Galopin, J. Bloch, A. Lemaître, P. T. Leung, P. Rousignol, R. Binder, J. Tignon, and S. Schumacher, *Scientific Reports* **3**, 3016 (2013).
- [16] S. M. H. Luk, P. Lewandowski, N. H. Kwong, E. Baudin, O. Lafont, J. Tignon, P. T. Leung, C. K. P. Chan, M. Babilon, S. Schumacher, and R. Binder, *J. Opt. Soc. Am. B* **35**, 146 (2018).
- [17] O. Lafont, S. M. H. Luk, P. Lewandowski, N. H. Kwong, P. T. Leung, E. Galopin, A. Lemaître, J. Tignon, S. Schumacher, E. Baudin, and R. Binder, *Applied Physics Letters* **110**, 061108 (2017).
- [18] F. P. Laussy, I. A. Shelykh, G. Malpuech, and A. Kavokin, *Phys. Rev. B* **73**, 035315 (2006).
- [19] O. Bleu, D. D. Solnyshkov, and G. Malpuech, *Phys. Rev. B* **95**, 115415 (2017).
- [20] K. Fang and Y. Wang, *Phys. Rev. Lett.* **122**, 233904 (2019).
- [21] C. Guo, M. Xiao, Y. Guo, L. Yuan, and S. Fan, *Phys. Rev. Lett.* **124**, 106103 (2020).
- [22] A. Kavokin, G. Malpuech, and M. Glazov, *Phys. Rev. Lett.* **95**, 136601 (2005).
- [23] S. Klemmt, T. H. Harder, O. A. Egorov, K. Winkler, R. Ge, M. A. Bandres, M. Emmerling, L. Worschech, T. C. H. Liew, M. Segev, C. Schneider, and S. Höfling, *Nature* **562**, 552 (2018).
- [24] A. Gianfrate, O. Bleu, L. Dominici, V. Ardizzone, M. De Giorgi, D. Ballarini, G. Lerario, K. West, L. Pfeiffer, D. Solnyshkov, D. Sanvitto, and G. Malpuech, *Nature* **578**, 381 (2020).
- [25] O. Bleu, D. D. Solnyshkov, and G. Malpuech, *Phys. Rev. B* **97**, 195422 (2018).
- [26] L. Polimeno, M. De Giorgi, G. Lerario, L. De Marco, L. Dominici, V. Ardizzone, M. Pugliese, C. T. Prontera, V. Maiorano, A. Moliterni, C. Giannini, V. Olieric, G. Gigli, D. Ballarini, D. Solnyshkov, G. Malpuech, and D. Sanvitto, arXiv preprint arXiv:2007.14945 (2020).
- [27] D. W. Berreman, *J. Opt. Soc. Am.* **62**, 502 (1972).
- [28] M. V. Berry, Proceedings of the Royal Society of London. A. Mathematical and Physical Sciences **392**, 45 (1984).
- [29] G. Panzarini, L. C. Andreani, A. Armitage, D. Baxter, M. Skolnick, V. Astratov, J. Roberts, A. V. Kavokin, M. R. Vladimirova, and M. Kaliteevski, *Physics of the Solid State* **41**, 1223 (1999).
- [30] A. A. Demenev, Y. V. Grishina, A. V. Larionov, N. A. Gippius, C. Schneider, S. Höfling, and V. D. Kulakovskii, *Phys. Rev. B* **96**, 155308 (2017).
- [31] M. Maragkou, C. E. Richards, T. Ostatnický, A. J. Grundy, J. Zajac, M. Hugues, W. Langbein, and P. G. Lagoudakis, *Optics letters* **36**, 1095 (2011).
- [32] F. Wilczek and A. Shapere, *Geometric phases in physics*, Vol. 5 (World Scientific, 1989).